Organic Light-Emitting Diodes on Solution-Processed Graphene Transparent Electrodes

Junbo Wu,[†] Mukul Agrawal,[‡] Héctor A. Becerril,[§] Zhenan Bao,[§] Zunfeng Liu,[⊥] Yongsheng Chen,[⊥] and Peter Peumans[‡,*]

[†]Department of Materials Science and Engineering, [‡]Department of Electrical Engineering, [§]Department of Chemical Engineering, Stanford University, Stanford, California 94305, and [⊥]Key Laboratory for Functional Polymer Materials and Center for Nanoscale Science & Technology, Institute of Polymer Chemistry, College of Chemistry, Nankai University, Tianjin 300071, P. R. China

ABSTRACT Theoretical estimates indicate that graphene thin films can be used as transparent electrodes for thin-film devices such as solar cells and organic light-emitting diodes, with an unmatched combination of sheet resistance and transparency. We demonstrate organic light-emitting diodes with solution-processed graphene thin film transparent conductive anodes. The graphene electrodes were deposited on quartz substrates by spin-coating of an aqueous dispersion of functionalized graphene, followed by a vacuum anneal step to reduce the sheet resistance. Small molecular weight organic materials and a metal cathode were directly deposited on the graphene anodes, resulting in devices with a performance comparable to control devices on indium—tin-oxide transparent anodes. The outcoupling efficiency of devices on graphene and indium—tin-oxide is nearly identical, in agreement with model predictions.

KEYWORDS: graphene · OLED · transparent conductor · outcoupling · solution-processed

Organic light-emitting diodes (OLEDs) are a promising electronic display and solid-state lighting technology because of their combination of high luminous efficiency and compatibility with a wide variety of substrates. Extensive research efforts[1−7] over the last two decades have resulted in improvements in the luminous efficiency, lifetime, and color gamut of both small molecular weight and polymer OLEDs since the introduction of the bilayer organic electroluminescent heterostructure diode by C. W. Tang.[8]

An important component of OLEDs is the transparent conductive electrode through which light couples out of the devices. Indium−tin-oxide (ITO) is traditionally used as transparent conductor, but has a number of disadvantages. First, ITO may be too expensive[9] for use in OLEDs for lighting because of the cost of indium and the low-throughput deposition process used. Second, metal oxides such as ITO (about 150 nm thick to ensure electrical performance) are brittle and therefore of limited use on flexible substrates.[10] Third, indium is known to diffuse into the active layers of OLEDs, which leads to a degradation of performance over time.[11] There is a clear need for alternative transparent electrodes whose optical and electrical performance is similar to that of ITO but without its drawbacks. Several alternative transparent electrodes have been demonstrated, including other transparent conductive oxides,[12,13] very thin metal films,[14] carbon nanotube (CNT) random meshes,[7,15] metal nanowire random meshes,[16] and metal gratings.[17] While substantial progress has been made, many issues remain to be addressed, such as performance, cost, lifetime, roughness, manufacturability, *etc.* In this work, we demonstrate OLEDs on transparent graphene electrodes, with a device performance that is competitive with that of control devices on ITO.

Graphene has promise as a transparent conductor because of its unique electronic structure.[18−20] In principle, charge carriers in an individual graphene sheet delocalize over the entire sheet and can travel thousands of interatomic distances without scattering. Since graphene is a zero-gap semiconductor with a very high Fermi velocity $v_F = 10^6$ m/s, individual graphene sheets have very high in-plane conductivities.[21] Graphene can be chemically doped at doping levels of $N_i = 10^{12}$ cm^{-2} while maintaining charge carrier mobilities of $\mu = 10^5$ cm^2/(V s) or higher.[20,22,23] Based on these values, the sheet resistance of graphene is

$$R_{sh} = \frac{1}{e\mu N_i N} = \frac{62.4\Omega}{N} \qquad (1)$$

where N is the number of monolayers of graphene. The sheet resistance of a

See the accompanying Perspective by Kumar and Zhou on p 11.

*Address correspondence to ppeumans@stanford.edu.

Received for review July 3, 2009 and accepted November 5, 2009.

Published online November 10, 2009. 10.1021/nn900728d

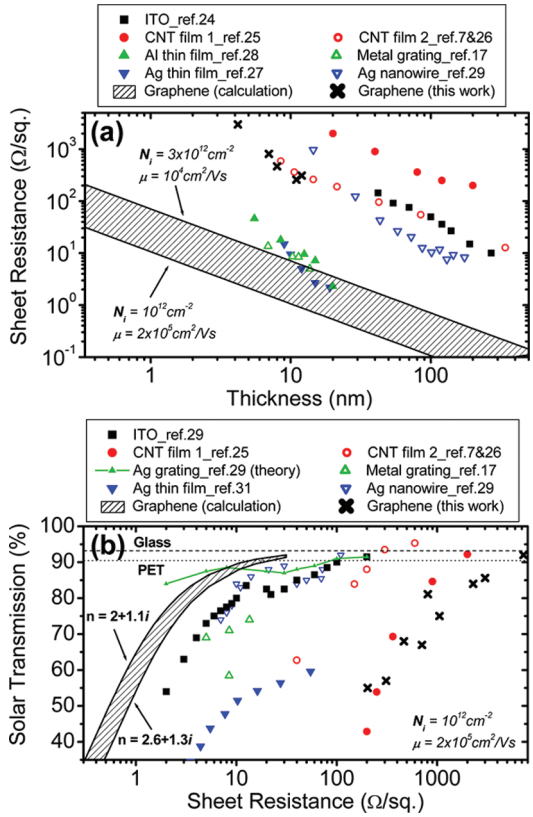

Figure 1. (a) Film thickness dependence of sheet resistance for different transparent conductors. Two limiting values were calculated for graphene using $\mu = 2 \times 10^5$ cm^2/(V s) at $N_i = 10^{12}$ cm^{-2} and $\mu = 10^4$ cm^2/(V s) at $N_i = 3 \times 10^{12}$ cm^{-2}. The thicknesses of the Ag nanowire film and metal grating are mean thicknesses obtained by spreading the mass of the metal over the entire substrate area. (b) Solar photon flux-weighted transmission *vs* sheet resistance for different transparent conductors. Two limiting lines of graphene film were calculated by using two different refractive indexes $n = 2.0 + 1.1i$ and $n = 2.6 + 1.3i$ for graphene, assuming $\mu = 2 \times 10^5$ cm^2/(V s) and $N_i = 10^{12}$ cm^{-2}. Two horizontal lines represent the transmission through bare glass (dashed line, $n = 1.463$) and PET (polyethylene terephthalate) (dotted line, $n = 1.575$) by including Fresnel reflections at both the air/(glass or PET) and (glass or PET)/air interfaces. Solar transmission is calculated by integrating the product of the spectrally resolved transmittance with the spectrally resolved AM1.5 photon flux over the spectral range of 400−800 nm.

graphene film is plotted as a function of film thickness (assuming that each graphene layer is 0.34 nm thick) in Figure 1a, and compared to experimental data for ITO thin films[24] and other recently developed alternative transparent electrodes such as CNT random meshes,[7,25,26] thin metal films,[27,28] metal gratings,[17] and Ag nanowire networks.[29] A range of resistivities was calculated for graphene films by using the limiting values for mobility and carrier density of $\mu = 2 \times 10^5$ cm^2/(V s) and $N_i = 10^{12}$ cm^{-2}, and $\mu = 10^4$ cm^2/(V s) and $N_i = 3 \times 10^{12}$ cm^{-2}.[22,30] To achieve a sheet resistance of 10Ω/□, >100 nm thick films of CNTs and ITO are needed. In contrast, <10 nm of graphene is in theory sufficient to achieve a sheet resistance <10Ω/□. Only metal thin films and gratings approach the sheet resistance of graphene for a thickness between 10 and 20 nm.

Figure 1b summarizes the optical transmission averaged over the 400−800 nm spectral range weighted by the AM1.5G solar spectrum, as a function of sheet resistance for different candidate transparent conductors for the structure air/glass/transparent conductor/air or air/polyethylene terephthalate (PET)/transparent conductor/air.[7,17,25,26,29,31] The sheet resistance of graphene was calculated as described above assuming $\mu = 2 \times 10^5$cm^2/(V s) and $N_i = 10^{12}$cm^{-2}. The transmission of graphene was calculated using the transfer matrix method[32] and spectrally averaged as described above. The literature reports a range of values for the optical properties of graphene, varying from $n = 2.0 + 1.1i$[33] to $n = 2.6 + 1.3i$[34,35] with the latter value being that of graphite. A range of transmissivities was calculated for graphene using these extreme values. This analysis shows that graphene has the potential to achieve a superior combination of sheet resistance and solar averaged optical transmission.

Various methods to make thin-films of graphene have been developed such as the scotch tape-method[18] and epitaxial growth,[36] but these methods are not suitable for low-cost, large-area applications. The graphene electrodes used in this work were deposited on quartz slides by spin-coating water-based dispersions of functionalized graphene (see Methods). The functionalized graphene material was prepared through a modified Hummers method as described elsewhere.[37,38] The resulting functionalized graphene films must be reduced, increasing both the light absorption and electrical conductivity of the film. High-temperature vacuum annealing was used here, which was shown to be more effective than chemical reduction methods.[38,39] The sheet resistance and solar transmittance of the resulting films are plotted in Figure 1a,b (crosses). The thickness of the graphene films used is ~7 nm, and the corresponding sheet resistance and transmission are ~800Ω/□ and 82% at 550 nm, respectively. The sheet resistance is >2 orders of magnitude higher than our theoretical estimates because large-area graphene films produced *via* solution processing of functionalized graphene contain multiple grain boundaries and incorporate lattice defects and oxidative traps that limit charge carrier transport.[40,41]

Graphene thin films have been used as an anode in dye-sensitized solar cells[42] and organic solar cells.[39,43,44] Electroluminescent thin-film devices have different requirements for the transparent electrode because both carrier injection and light outcoupling must be considered. OLEDs on ITO benefit from optical interference effects in the ITO layer to control the outcoupling efficiency and radiation pattern.[45−47] Here, we demonstrated OLEDs on graphene thin films with electrical and optical performance comparable to that of control devices on ITO.

Basic OLED structures were fabricated on graphene films on quartz and on commercially obtained 130 nm-

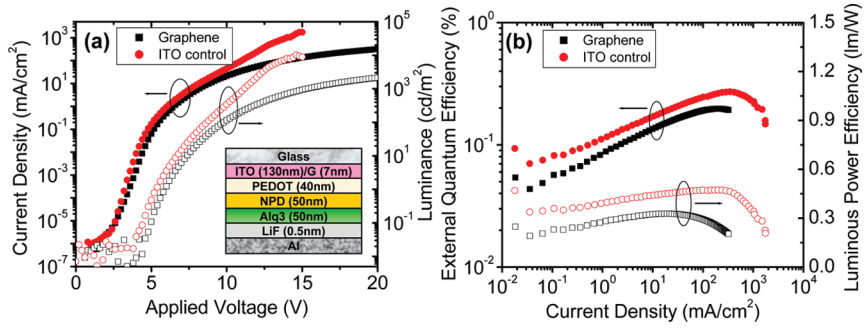

Figure 2. (a) Current density (filled symbols) and luminance (open symbols) *vs* applied forward bias for an OLED on graphene (squares) and ITO (circles), with OLED device structure anode/PEDOT:PSS/NPD(50 nm)/Alq_3(50 nm)/LiF/Al as shown in the inset. (b) External quantum efficiency (EQE) (filled symbols) and luminous power efficiency (LPE) (open symbols) for an OLED on graphene film (squares) and ITO glass (circles). The luminance, EQE, and LPE were adjusted to reflect total front emission power according to the method described in the Methods.

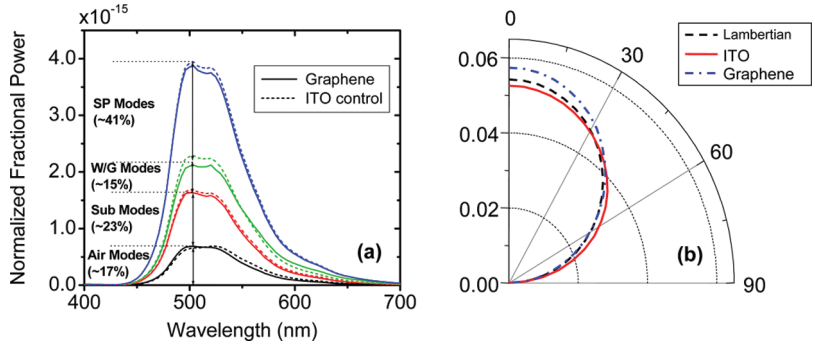

Figure 3. (a) Simulated angularly integrated spectral density of emitted power into unbound (UB) air modes, substrate-trapped (ST) modes, wave-guided (WG) modes, and surface plasmon polariton (SPP) modes. (b) Simulated spectrally integrated emitted power per unit solid angle for OLEDs on graphene film (blue dash-dotted line) and control ITO (red solid line) glass. A Lambertian response (black dashed line) is plotted for reference.

thick ITO on glass (sheet resistance $<20\Omega$/sq), with the device structure: anode/poly(3,4-ethylenedioxythiophene) poly(styrenesulfonate) (PEDOT:PSS)/*N*,*N*′-di-1-naphthyl-*N*,*N*′-diphenyl-1,1′-biphenyl-4,4′diamine (NPD) (50 nm)/tris(8-hydroxyquinoline) aluminum (Alq_3) (50 nm)/lithium fluoride (LiF) (0.3 nm)/Al, as shown in the inset of Figure 2a. Figure 2a shows the current density and luminance as a function of applied forward bias for typical devices. OLEDs on graphene have a current drive and light emission intensity comparable to control devices on ITO for current densities <10 mA/cm^2. At current densities >10 mA/cm^2, the sheet resistance of graphene leads to a voltage drop in the electrode. Luminance was measured by a flat calibrated silicon photodetector that captures 67% of the emitted light (see Methods). The OLED turn-on voltage (defined at 0.02 cd/m^2) is 4.5 and 3.8 V, and it reaches a luminance of 300 cd/m^2 at 11.7 and 9.9 V, for graphene and ITO anodes, respectively.

In Figure 2b, the external quantum efficiency (EQE) and luminous power efficiency (LPE) of both graphene-based and ITO-based OLEDs are shown. The graphene-based OLED performance nearly matches that of the ITO control device despite the higher sheet resistance and different workfunction[39] of the graphene anode. The conductive PEDOT:PSS layer further removes the effects of small differences in workfunction that may exist between ITO and graphene.

The nearly identical EQE is surprising because the fraction of optical power that couples out of an OLED structure depends strongly on the thickness of the various layers.[48,49] The angular and spectral distribution of light emitted from the organic active layer was modeled as described elsewhere.[50] Figure 3a shows the simulated optical power emitted into unbound (UB) air modes, substrate trapped (ST) modes, waveguided (WG) modes, and surface plasmon polariton (SPP) modes at the metal cathode/organic interface, and Table 1 summaries the detailed simulation results. The fraction of photons emitted into UB modes is the outcoupling efficiency. When spectrally integrated, we find that 17% of the optical power couples out for this OLED structure on both graphene and ITO, despite the differences in layer structure.[47] Figure 3b shows the calculated spectrally integrated power density of emitted radiation per unit solid angle into UB optical

TABLE 1. Simulated Fraction of Emitted Optical Power into the Various Modes Supported by the OLED Structures

	air modes	ST modes	WG modes	SPP modes	anode absorption	metal absorption
graphene	16.54%	22.86%	15.15%	40.54%	4.01%	0.90%
ITO	17.05%	23.51%	14.59%	40.77%	3.19%	0.88%

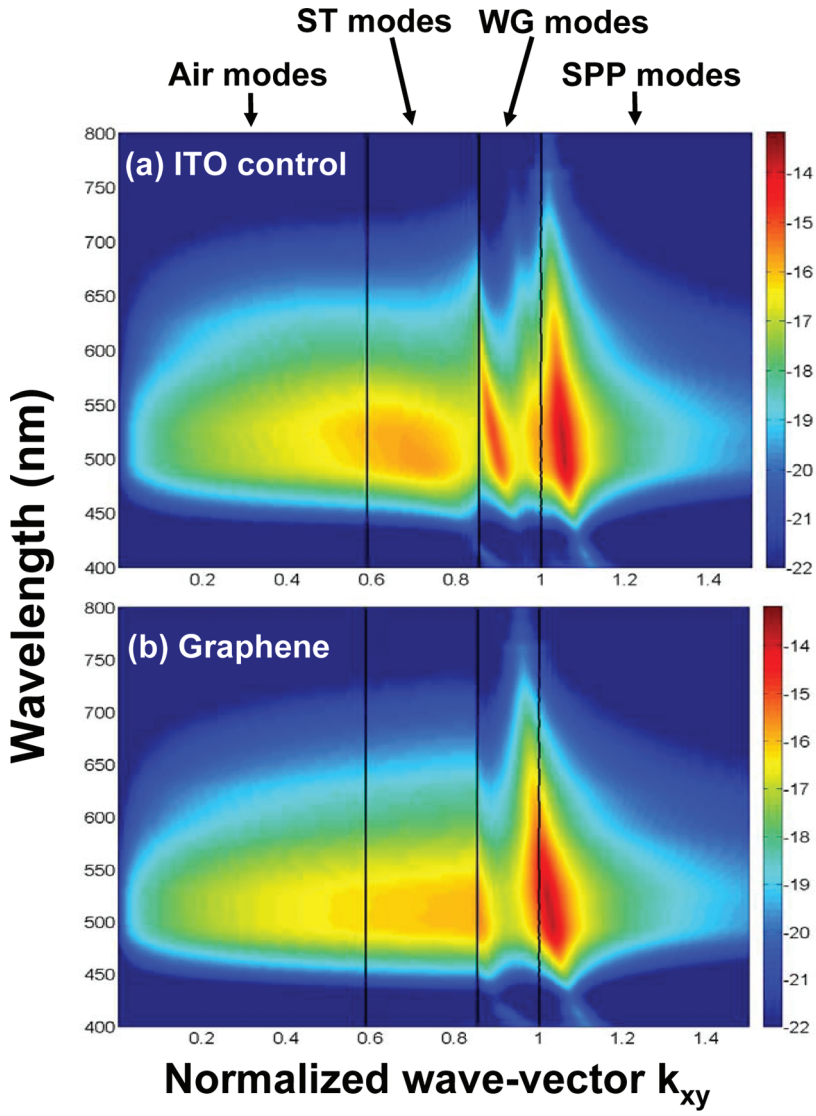

Figure 4. The fraction of power emitted as a function of normalized in-plane wave-vector k_{xy} for all wavelengths between 400 and 800 nm for an OLED on ITO (a) and graphene (b), with device structure anode/PEDOT:PSS/NPD(50 nm)/Alq_3(50 nm)/LiF/Al as shown in the inset of Figure 2a. The fraction of power coupled to air modes, substrate modes, wave-guided modes, and surface plasmon polariton modes is evaluated by integrating the power distribution over the appropriate ranges of the in-plane wave-vector $\mathbf{k}_{xy}$.

modes at different azimuthal angles from the surface normal. The emission pattern is nearly Lambertian for both graphene and ITO-based OLEDs.

Figure 4 shows the simulated fraction of power emitted as a function of wavelength and normalized in-plane wavevector $\mathbf{k}_{xy}$ for the OLED structure on graphene and ITO (assuming a glass substrate). While the fraction of power emitted into the various modes is nearly identical for devices on graphene and ITO (Figure 3a), the power distribution patterns within each layer are quite different because of the differences in layer structure. Specifically, the OLED structure on graphene does not support a WG mode due to the thin overall dielectric structure.

In conclusion, we demonstrated that graphene thin films can be used as transparent conductive anode in OLEDs. The graphene thin films were prepared by solution processing of functionalized graphene followed by a reduction step to improve the conductivity. The electrical and optical performance of a small molecule OLED on graphene is similar to that of control devices on ITO despite marked differences in the total thickness of the optical stack. The graphene film used in this work is ~7 nm thick and consists mostly of multiple layers of graphene. The film roughness is <3 nm, which is adequate for use as an anode in OLEDs and organic solar cells. Both transmittance and sheet resistance decrease with increasing film thickness. Thicker graphene film would help reduce the sheet resistance but the increased optical absorption due to the thicker film would decrease the photon outcoupling efficiency. Further optimization of the graphene film quality and thickness may lead to improved device performance. For graphene to become a viable alternative to ITO, further work is needed to develop methods to deposit high-quality, thin layers of graphene on low-cost plastic substrates in a cost-effective manner.[51,52]

METHODS

Graphene Film Preparation. A graphite crystal was chemically oxidized by treatment with various solutions of $NaNO_3$, $KMnO_4$, concentrated H_2SO_4, and 30 wt % H_2O_2, washed with HCl and purified water, and ultrasonicated to exfoliate individual graphene oxide sheets. This procedure produces a loose brown powder which can be dispersed in water at loadings of up to ~15 mg/mL. The graphene electrodes used in this work were deposited on quartz slides by spin-coating dispersions of functionalized graphene in water. The spin-coating rate was increased every 30 s from an initial value of 500−800 rpm to gradually spread the water dispersion on the quartz, and finally to 1600 rpm to dry the film. Residual water was removed by heating the films to 100 °C in a vacuum oven for several hours. The resulting functionalized graphene films were reduced by vacuum annealing at 1100 °C for 3 h.

OLED Device Fabrication. Small molecule organic light-emitting diodes were fabricated on graphene films on quartz and on commercially obtained 130 nm-thick ITO on glass (sheet resistance <20Ω/sq) as transparent anode. The ITO substrates were cleaned in acetone, and isopropyl alcohol followed by UV-ozone treatment for 15 min. Poly(3,4-ethylenedioxythio- phene)poly(styrenesulfonate) (PEDOT:PSS) was spin-coated on both graphene and ITO substrates followed by annealing in an N_2 glovebox for 20 min. All organic materials were obtained commercially and then purified using thermal gradient sublimation at least twice. The organic thin films and metal cathode were deposited at room temperature by thermal evaporation in high vacuum (~10^{-7} Torr). The deposi-

tion rate is 1−2 Å/s for organic materials, and 4−5 Å/s for metal cathode. The layer structure of the devices is anode/poly(3,4-ethylenedioxythiophene) poly(styrenesulfonate) (PEDOT:PSS)/*N,N′*-di-1-naphthyl-*N,N′*-diphenyl-1,1′-biphenyl-4,4′diamine (NPD)/tris(8-hydroxyquinoline) aluminum (Alq_3)/lithium fluoride (LiF)/Al. The Al cathode was deposited through a shadow mask with 1 mm diameter circular openings.

Measurements. Current−voltage characteristics were measured using an HP 4145B semiconductor parameter analyzer. Luminance was measured by a flat calibrated silicon photodiode that captures light emitted within a cone of 55°, and then adjusted to include uncaptured emissive power. For a Lambertian emission source, the power emitted within a cone is

$$P_\Omega = \int_0^{2\pi} \int_0^{\theta} \cos\theta' \sin\theta' \, d\theta' \, d\phi = \frac{\pi}{2}(1 - \cos 2\theta)$$

The fraction of optical power emitted by the OLED that is captured by our photodiode is

$$\frac{P_{55°}}{P_{90°}} = \frac{(1 - \cos(110°))}{(1 - \cos(180°))} = 67\%$$

The luminous power reported is the value measured by the photodiode (corrected for the spectral response of the photodiode), and then divided by the fraction captured (67%).

Acknowledgment. This work was supported by the National Science Foundation, the Global Climate and Energy Project at Stanford (GCEP), and the Center for Advanced Molecular Photovoltaics (CAMP) (Award No KUS-C1-015-21), made by King Abdullah University of Science and Technology (KAUST).

REFERENCES AND NOTES

1. Baldo, M. A.; O'Brien, D. F.; You, Y.; Shoustikov, A.; Sibley, S.; Thompson, M. E.; Forrest, S. R. Highly Efficient Phosphorescent Emission from Organic Electroluminescent Devices. *Nature* **1998**, *395*, 151–154.
2. Sun, Y.; Giebink, N. C.; Kanno, H.; Ma, B.; Thompson, M. E.; Forrest, S. R. Management of Singlet and Triplet Excitons for Efficient White Organic Light-Emitting Devices. *Nature* **2006**, *440*, 908–912.
3. D'Andrade, B. W.; Holmes, R. J.; Forrest, S. R. Efficient Organic Electrophosphorescent White-Light-Emitting Device with a Triple Doped Emissive Layer. *Adv. Mater.* **2004**, *16*, 624–628.
4. Burroughes, J. H.; Bradley, D. D. C.; Brown, A. R.; Marks, R. N.; Mackay, K.; Friend, R. H.; Burns, P. L.; Holmes, A. B. Light-Emitting Diodes Based on Conjugated Polymers. *Nature* **1990**, *347*, 539–541.
5. Friend, R. H.; Gymer, R. W.; Holmes, A. B.; Burroughes, J. H.; Marks, R. N.; Taliani, C.; Bradley, D. D. C.; Santos, D. A. D.; Bredas, J. L.; Logdlund, M.; Salaneck, W. R. Electroluminescence in Conjugated Polymers. *Nature* **1999**, *397*, 121–128.
6. He, G.; Pfeiffer, M.; Leo, K.; Hofmann, M.; Birnstock, J.; Pudzich, R.; Salbeck, J. High-Efficiency and Low-Voltage p-i-n Electrophosphorescent Organic Light-Emitting Diodes with Double-Emission Layers. *Appl. Phys. Lett.* **2004**, *85*, 3911–3913.
7. Li, J.; Hu, L.; Wang, L.; Zhou, Y.; Gruner, G.; Marks, T. J. Organic Light-Emitting Diodes Having Carbon Nanotube Anodes. *Nano Lett.* **2006**, *6*, 2472–2477.
8. Tang, C. W.; VanSlyke, S. A. Organic Electroluminescent Diodes. *Appl. Phys. Lett.* **1987**, *51*, 913–915.
9. Forrest, S. R. The Path to Ubiquitous and Low-Cost Organic Electronic Appliances on Plastic. *Nature* **2004**, *428*, 911–918.
10. Chen, Z.; Cotterell, B.; Wang, W.; Guenther, E.; Chua, S. A Mechanical Assessment of Flexible Optoelectronic Devices. *Thin Solid Films* **2001**, *394*, 201–205.
11. Lee, S. T.; Gao, Z. Q.; Hung, L. S. Metal Diffusion from Electrodes in Organic Light-Emitting Diodes. *Appl. Phys. Lett.* **1999**, *75*, 1404–1406.
12. Kim, H.; Gilmore, C. M.; Horwitz, J. S.; Pique, A.; Murata, H.; Kushto, G. P.; Schlaf, R.; Kafafi, Z. H.; Chrisey, D. B. Transparent Conducting Aluminum-Doped Zinc Oxide Thin Films for Organic Light-Emitting Devices. *Appl. Phys. Lett.* **2000**, *76*, 259–261.
13. Cui, J.; Wang, A.; Edleman, N. L.; Ni, J.; Lee, P.; Armstrong, N. R.; Marks, T. J. Indium Tin Oxide Alternatives—High Work Function Transparent Conducting Oxides as Anodes for Organic Light-Emitting Diodes. *Adv. Mater.* **2001**, *13*, 1476–1480.
14. Pode, R. B.; Lee, C. J.; Moon, D. G.; Han, J. I. Transparent Conducting Metal Electrode for Top Emission Organic Light-Emitting Devices: Ca−Ag double layer. *Appl. Phys. Lett.* **2004**, *84*, 4614–4616.
15. Zhang, D.; Ryu, K.; Liu, X.; Polikarpov, E.; Ly, J.; Tompson, M. E.; Zhou, C. Transparent, Conductive, and Flexible Carbon Nanotube Films and Their Application in Organic Light-Emitting Diodes. *Nano Lett.* **2006**, *6*, 1880–1886.
16. Lee, J.-Y.; Peumans, P. Unpublished.
17. Kang, M.-G.; Guo, L. J. Nanoimprinted Semitransparent Metal Electrodes and Their Application in Organic Light-Emitting Diodes. *Adv. Mater.* **2007**, *19*, 1391–1396.
18. Novoselov, K. S.; Geim, A. K.; Morozov, S. V.; Jiang, D.; Zhang, Y.; Dubonos, S. V.; Grigorieva, I. V.; Firsov, A. A. Electric Field Effect in Atomically Thin Carbon Films. *Science* **2004**, *306*, 666–669.
19. Zhang, Y.; Tan, Y.; Stormer, H. L.; Kim, P. Experimental Observation of the Quantum Hall Effect and Berry'S Phase in Graphene. *Nature* **2005**, *438*, 201–204.
20. Geim, A. K.; Novoselov, K. S. The Rise of Graphene. *Nat. Mater.* **2007**, *6*, 183–191.
21. Fang, T.; Konar, A.; Xing, H.; Jena, D. Carrier Statistics and Quantum Capacitance of Graphene Sheets and Ribbons. *Appl. Phys. Lett.* **2007**, *91*, 092109.
22. Schedin, F.; Geim, A. K.; Morozov, S. V.; Hill, E. W.; Blake, P.; Katsnelson, M. I.; Novoselov, K. S. Detection of Individual Gas Molecules Adsorbed on Graphene. *Nat. Mater.* **2007**, *6*, 652–655.
23. Chen, J.; Jang, C.; Xiao, S.; Ishigami, M.; Fuhrer, M. S. Intrinsic and Extrinsic Performance Limits of Graphene Devices on SiO_2. *Nat. Nano* **2008**, *3*, 206–209.
24. Kim, D.; Park, M.; Lee, H.; Lee, G. Thickness Dependence of Electrical Properties of ITO Film Deposited on a Plastic Substrate by RF Magnetron Sputtering. *Appl. Surf. Sci.* **2006**, *253*, 409–411.
25. Kymakis, E.; Stratakis, E.; Koudoumas, E. Integration of Carbon Nanotubes As Hole Transport Electrode in Polymer/Fullerene Bulk Heterojunction Solar Cells. *Thin Solid Films* **2007**, *515*, 8598–8600.
26. Gruner, G. Carbon Nanotube Films for Transparent and Plastic Electronics. *J. Mater. Chem.* **2006**, *16*, 3533–3539.
27. O'Connor, B.; Haughn, C.; An, K.; Pipe, K. P.; Shtein, M. Transparent and Conductive Electrodes Based on Unpatterned, Thin Metal Films. *Appl. Phys. Lett.* **2008**, *93*, 223304.
28. Camacho, J. M.; Oliva, A. I. Surface and Grain Boundary Contributions in the Electrical Resistivity of Metallic Nanofilms. *Thin Solid Films* **2006**, *515*, 1881–1885.
29. Lee, J.-Y.; Connor, S. T.; Cui, Y.; Peumans, P. Solution-Processed Metal Nanowire Mesh Transparent Electrodes. *Nano Lett.* **2008**, *8*, 689–692.
30. Bolotin, K. I.; Sikes, K. J.; Jiang, Z.; Klima, M.; Fudenberg, G.; Hone, J.; Kim, P.; Stormer, H. L. Ultrahigh Electron Mobility in Suspended Graphene. *Solid State Commun.* **2008**, *146*, 351–355.
31. Charton, C.; Fahland, M. Optical Properties of Thin Ag Films Deposited by Magnetron Sputtering. *Surf. Coat. Technol.* **2003**, *174−175*, 181–186.
32. Heavens, O. S. *Optical Properties of Thin Solid Films*; Dover: New York, 1965; pp 46−95.
33. Ni, Z. H.; Wang, H. M.; Kasim, J.; Fan, H. M.; Yu, T.; Wu, Y. H.; Feng, Y. P.; Shen, Z. X. Graphene Thickness Determination Using Reflection and Contrast Spectroscopy. *Nano Lett.* **2007**, *7*, 2758–2763.

34. Blake, P.; Hill, E. W.; Neto, A. H. C.; Novoselov, K. S.; Jiang, D.; Yang, R.; Booth, T. J.; Geim, A. K. Making Graphene Visible. *Appl. Phys. Lett.* **2007**, *91*, 063124.
35. Nair, R. R.; Blake, P.; Grigorenko, A. N.; Novoselov, K. S.; Booth, T. J.; Stauber, T.; Peres, N. M. R.; Geim, A. K. Fine Structure Constant Defines Visual Transparency of Graphene. *Science* **2008**, *320*, 1308.
36. Rollings, E.; Gweon, G.-H.; Zhou, S. Y.; Mun, B. S.; McChesney, J. L.; Hussain, B. S.; Fedorov, A. V.; First, P. N.; de Heer, W. A.; Lanzara, A. Synthesis and Characterization of Atomically Thin Graphite Films on a Silicon Carbide Substrate. *J. Phys. Chem. Solids* **2006**, *67*, 2172–2177.
37. Hummers, W. S.; Offeman, R. E. Preparation of Graphitic Oxide. *J. Am. Chem. Soc.* **1958**, *80*, 1339.
38. Becerril, H. A.; Mao, J.; Liu, Z.; Stoltenberg, R. M.; Bao, Z.; Chen, Y. Evaluation of Solution-Processed Reduced Graphene Oxide Films as Transparent Conductors. *ACS Nano* **2008**, *2* (3), 463–470.
39. Wu, J.; Becerril, H. A.; Bao, Z.; Liu, Z.; Chen, Y.; Peumans, P. Organic Solar Cells with Solution-Processed Graphene Transparent Electrodes. *Appl. Phys. Lett.* **2008**, *92*, 263302.
40. Mkhoyan, K. A.; Contryman, A. W.; Silcox, J.; Stewart, D. A.; Eda, G.; Mattevi, C.; Miller, S.; Chhowalla, M. Atomic and Electronic Structure of Graphene-Oxide. *Nano Lett.* **2009**, *9*, 1058–1063.
41. Mattevi, C.; Eda, G.; Agnoli, S.; Miller, S.; Mkhoyan, K. A.; Celik, O.; Mastrogiovanni, D.; Granozzi, G.; Garfunkel, E.; Chhowalla, M. Evolution of Electrical, Chemical, and Structural Properties of Transparent and Conducting Chemically Derived Graphene Thin Films. *Adv. Funct. Mater.* **2009**, *19*, 1–7.
42. Wang, X.; Zhi, L.; Mullen, K. Transparent, Conductive Graphene Electrodes for Dye-Sensitized Solar Cells. *Nano Lett.* **2008**, *8*, 323–327.
43. Eda, G.; Lin, Y.; Miller, S.; Chen, C.; Su, W.; Chhowalla, M. Transparent and Conducting Electrodes for Organic Electronics from Reduced Graphene Oxide. *Appl. Phys. Lett.* **2008**, *92*, 233305.
44. Tung, V. C.; Chen, L.; Allen, M. J.; Wassei, J. K.; Nelson, K.; Kaner, R. B.; Yang, Y. Low-Temperature Solution Processing of Graphene−Carbon Nanotube Hybrid Materials for High-Performance Transparent Conductors. *Nano Lett.* **2009**, *9*, 1949–1955.
45. Greenham, N. C.; Friend, R. H.; Bradley, D. D. C. Angular Dependence of the Emission from a Conjugated Polymer Light-Emitting Diode: Implications for Efficiency Calculations. *Adv. Mater.* **1994**, *6*, 491–494.
46. Madigan, C. F.; Chen, L.-M.; Sturm, J. C. Improvement of Output Coupling Efficiency of Organic Light-Emitting Diodes by Backside Substrate Modification. *Appl. Phys. Lett.* **2000**, *76*, 1650–1652.
47. Agrawal, M.; Sun, Y.; Forrest, S. R.; Peumans, P. Enhanced Outcoupling from Organic Light-Emitting Diodes Using Aperiodic Dielectric Mirrors. *Appl. Phys. Lett.* **2007**, *90*, 241112.
48. D'Andrade, B. W.; Brown, J. J. Organic Light-Emitting Device Luminaire for Illumination Applications. *Appl. Phys. Lett.* **2006**, *88*, 192908.
49. Lu, M.-H.; Weaver, M. S.; Zhou, T. X.; Rothman, M.; Kwong, R. C.; Hack, M.; Brown, J. J. High-Efficiency Top-Emitting Organic Light-Emitting Devices. *Appl. Phys. Lett.* **2002**, *81*, 3921–3923.
50. Agrawal, M.; Peumans, P. Design of Nonperiodic Dielectric Stacks for Tailoring the Emission of Organic Lighting-Emitting Diodes. *Opt. Express* **2007**, *15*, 9715–9721.
51. Kim, K. S.; Zhao, Y.; Jang, H.; Lee, S. Y.; Kim, J. M.; Kim, K. S.; Ahn, J.; Kim, P.; Choi, J.; Hong, B. H. Large-Scale Pattern Growth of Graphene Films for Stretchable Transparent Electrodes. *Nature* **2009**, *457*, 706–710.
52. Reina, A.; Jia, X.; Ho, J.; Nezich, D.; Son, H.; Bulovic, V.; Dresselhaus, M. S.; Kong, J. Large Area, Few-Layer Graphene Films on Arbitrary Substrates by Chemical Vapor Deposition. *Nano Lett.* **2009**, *9*, 30–35.